LANGMUIR Article
Cite This: Langmuir 2018, 34, 12764−12775
pubs.acs.org/Langmuir

DLVO Interaction Energies for Hollow Particles: The Filling Matters

Chongyang Shen,[†] Scott A. Bradford,[*,‡] Markus Flury,[§] Yuanfang Huang,[†] Zhan Wang,[∥] and Baoguo Li[*,†]

[†]Department of Soil and Water Sciences, College of Resources and Environmental Sciences, China Agricultural University, No. 2 Yuanmingyuan West Road, Haidian District, Beijing 100193, China

[‡]USDA, ARS, U.S. Salinity Laboratory, 450 West Big Springs Road, Riverside, California 92507-4617, United States

[§]Department of Crop and Soil Sciences, Washington State University, 2606 W Pioneer, Puyallup, Washington 98371, United States

[∥]College of Land and Environment, Shenyang Agricultural University, No. 120 Dongling Road, Shenhe District, Shenyang, Liaoning 110866, China

Supporting Information

ABSTRACT: A thorough knowledge of the interaction energy between a hollow particle (HP) and a surface or between two HPs is critical to the optimization of HP-based products and assessing the environmental risks of HPs and HP-associated pollutants. The van der Waals (vdW) energy between a HP and a surface is often calculated by subtracting the vdW energies of the inner and outer HP geometries. In this study, we show that this subtraction method is only valid when the interior and exterior fluids are the same, for example, for water-filled HPs (WHPs) dispersed in an aqueous solution. Expressions were developed to calculate the vdW energies for HPs whose interiors were filled with air (AHPs). The vdW energies were then calculated between a planar surface and a spherical or cylindrical WHP and AHP, and between WHPs or AHPs. The vdW attraction between a surface and a WHP was decreased at large separation distances compared to solid particles, and this reduced the depth of the secondary minimum. In contrast, the vdW attraction for AHPs and a surface was significantly reduced at all separation distances, and even became repulsive for thin shells, and this inhibited both primary and secondary minimum interactions. The vdW attraction between WHPs decreased with increasing shell thicknesses, and this reduced aggregation in both primary and secondary minima. In contrast, aggregation of AHPs was increased in both minima with decreasing shell thicknesses because of an increase in vdW attraction. Our theoretical calculations show the evolution of vdW and total interaction energies for HPs with different interior fluids and shell thicknesses. These results help explain various experimental observations such as inhibited attachment and favorable aggregation for AHPs (e.g., carbon nanotubes) and favorable bubble coalescence.

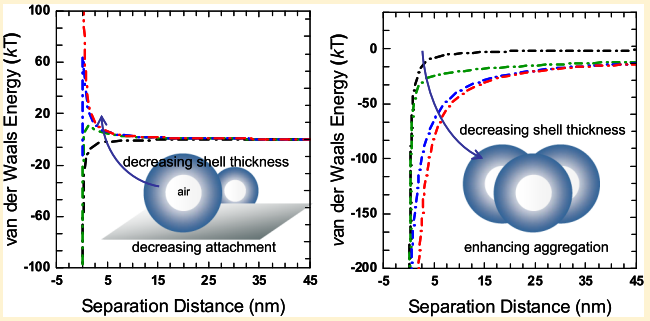

INTRODUCTION

Hollow particles (HPs) have attracted considerable interest for the past few decades because of their fascinating properties such as large surface area, low density, and high loading capacity.[1] For example, carbon nanotubes (CNTs) are typical HPs of cylindrical shape that were discovered a few years after the spherical Buckminsterfullerene in 1985.[2] CNTs possess unique electronic, mechanic, and structural properties, which make them particularly useful in technological applications.[3] Examples include drug delivery, coatings and films, energy storage, biosensors, and water treatment.[4] In addition to cylindrical CNTs, spherical HPs have found wide applications as catalysts, in lithium-ion batteries, and in minireactors.[5,6]

Some applications of HPs require their attachment on the surfaces of bulk materials which is controlled by interaction energies/forces.[7,8] A thorough understanding of the HP−surface interaction energies is therefore critical to the creation and optimization of HP-based products. In addition, the wide production and application of HPs will inevitably lead to their release into subsurface environments such as soil and sediments.[9] Some HPs can strongly absorb pollutants[10,11] and transport them in porous media (i.e., colloid-facilitated transport of contaminants).[12−14] The transport of HPs and HP-associated pollutants in the porous media is primarily controlled by HP interactions on collector surfaces.[15] Hence, the knowledge of HP−collector surface interaction energies is of importance to prevent groundwater from being contaminated by the HP-associated pollutants.

The Derjaguin−Landau−Verwey−Overbeek (DLVO) theory predicts that the interaction energy between a colloidal particle and a surface is dependent on van der Waals (vdW) attraction and electrical double-layer (DL) interaction. DLVO

Received: July 27, 2018
Revised: September 30, 2018
Published: October 8, 2018

DOI: 10.1021/acs.langmuir.8b02547
Langmuir 2018, 34, 12764−12775

theory is frequently extended to include short-range repulsion such as hydration and steric repulsion.[16,17] Existing theoretical studies[8,18] describe HP interactions by using a subtraction method to calculate the vdW energy (U_{vdW}) as vdW attraction is a volume force. Specifically, the vdW energy between a HP and a surface has been taken as $U_{vdW}^{out} - U_{vdW}^{in}$, where U_{vdW}^{out} and U_{vdW}^{in} are the vdW energies for the exterior and interior geometries, respectively, of a solid particle (SP) with the same composition as that of the HP shell. These calculations showed that hollowing an SP leads to a significant reduction of the vdW attraction only when the separation distance between the HP and the surface is large. Therefore, increasing the size of the hollow interior of the HP can significantly reduce secondary-minimum depth (U_{sec}) but has a minor influence on interaction energy barrier (U_{max}) and primary-minimum depth (U_{pri}). In contrast to the vdW force, the DL interaction and short-range forces such as hydration are surface forces which are not affected by the interior surface of the HP if the interior is isolated from the bulk solution.

In this work, the Hamaker approach[19] is used to show that the aforementioned subtraction method is valid for calculating vdW energies only for HPs when the interior and exterior fluids are the same (e.g., water-filled HP, denoted as WHPs). Furthermore, we develop expressions that can be used to calculate vdW energies for HPs whose interiors are filled with air (AHPs). We demonstrate that because of the reduced attraction to a collector, the mobility of AHPs in the environment can be enhanced in comparison to WHPs and especially SPs. The primary and secondary energy wells and attachment can disappear for AHPs when their shells are thin. These theoretical results are supported by experimental observations in the literature.[9,20−22] Although the aggregation of WHPs is inhibited compared to SPs, the aggregation of AHPs is enhanced. Our work theoretically advances the calculation of the interaction energy for HPs, and the findings have important implications for industrial applications and environmental risks of HPs.

THEORY

DLVO Interaction Energies for WHPs and AHPs. When evaluating the vdW interaction energy between an SP and a solid collector in water, we have to consider not only the SP and the collector but also a particle and a collector of the same sizes but consisting of water. We denote as follows:

U_{PC} = the vdW energy between the SP (subscript P) and the solid collector (subscript C) in vacuum.

U_{PW} = the vdW energy between the SP and the water collector (subscript W) in vacuum.

U_{WC} = the vdW energy between the water particle and the solid collector in vacuum.

U_{WW} = the vdW energy between the water particle and the water collector in vacuum.

U_P = the vdW energy for the SP in water at infinity.

U_w = the vdW energy for the water particle in water at infinity.

U_C = the vdW energy for the solid collector in water at infinity.

Values of U_{PC}, U_{PW}, U_{WC}, and U_{WW} are functions of separation distance between the SP and the collector, whereas U_P and U_C are constants. When the SP is brought from infinity to the neighborhood of the solid collector, the energy of the particle will change from U_P to $U_P + U_{PC} - U_{PW}$. Note that while bringing the SP toward the solid collector, we have to move a water particle toward infinity at the same time. The corresponding energy of the water particle will change from $U_W + U_{WC} - U_{WW}$ to U_W. Therefore, the vdW energy between the SP and the solid collector (i.e., the energy change due to variation in separation distance between them) in water is

$$U_{vdW} = U_{PC} + U_{WW} - U_{PW} - U_{WC} \quad (1)$$

According to eq 1, the value of vdW energy between the outer particle of a HP and the collector U_{vdW}^{out} can be written as

$$U_{vdW}^{out} = U_{PC}^{out} + U_{WW}^{out} - U_{PW}^{out} - U_{WC}^{out} \quad (2)$$

The expression used to calculate the vdW energy between the inner particle of the HP and the collector U_{vdW}^{in} is

$$U_{vdW}^{in} = U_{PC}^{in} + U_{WW}^{in} - U_{PW}^{in} - U_{WC}^{in} \quad (3)$$

The expression used to calculate the vdW energy U_{vdW} between a WHP and a solid collector in water thus is

$$\begin{aligned} U_{vdW} &= (U_{PC}^{out} - U_{PC}^{in}) + (U_{WW}^{out} - U_{WW}^{in}) - (U_{PW}^{out} - U_{PW}^{in}) \\ &\quad - (U_{WC}^{out} - U_{WC}^{in}) \\ &= U_{vdW}^{out} - U_{vdW}^{in} \end{aligned} \quad (4)$$

Equation 4 was adopted in the literature[8,18] for vdW energy calculations. It shows that the vdW energy for the WHP becomes zero in the limit when the inner particle size approaches that of the outer particle, that is, the particle becomes a complete water particle.

If the interior of the HP is vacuum, the vdW energy between the HP and the solid collector in water has to be calculated using the following expression:

$$\begin{aligned} U_{vdW} &= (U_{PC}^{out} - U_{PC}^{in}) + U_{WW}^{out} - (U_{PW}^{out} - U_{PW}^{in}) - U_{WC}^{out} \\ &= U_{vdW}^{out} - U_{vdW}^{in} + U_{WW}^{in} - U_{WC}^{in} \end{aligned} \quad (5)$$

The difference between eqs 4 and 5 is that $U_{WW}^{out} - U_{WW}^{in}$ and $U_{WC}^{out} - U_{WC}^{in}$ are adopted in the former equation, whereas U_{WW}^{out} and U_{WC}^{out} are used in the latter equation. This is because when bringing the WHP toward the solid collector, we at the same time only cause a hollow water particle (i.e., with the same shape as that of the solid part of the HP) to move toward infinity. In contrast, when we bring the HP with vacuum interior toward the solid collector, we at the same time cause a nonhollow water particle (with the same size as that of the outer particle) to move toward infinity.

The vdW energy between an AHP and a solid collector in water can be calculated by the follow equation:

$$\begin{aligned} U_{vdW} &= (U_{PC}^{out} - U_{PC}^{in} + U_{PC}^{in,air}) + U_{WW}^{out} \\ &\quad - (U_{PW}^{out} - U_{PW}^{in} + U_{PW}^{in,air}) - U_{WC}^{out} \\ &= U_{vdW}^{out} - U_{vdW}^{in} + U_{WW}^{in} - U_{WC}^{in} + U_{PC}^{in,air} - U_{PW}^{in,air} \end{aligned} \quad (6)$$

where $U_{PC}^{in,air}$ or $U_{PW}^{in,air}$ is the vdW energy between the air particle of the AHP and the solid collector or the water collector in vacuum. $U_{PC}^{in,air}$ and $U_{PW}^{in,air}$ can be omitted in eq 6 because the vdW energy, which is proportional to the atomic densities of the interacting bodies,[19] of air is so much lower than those of water and solids. Consequently, the expressions used to calculate the vdW energy for the HP with air and vacuum inside yield the same results. Equation 5 was used later in the paper for calculating the vdW energies for AHPs.

DOI: 10.1021/acs.langmuir.8b02547
Langmuir 2018, 34, 12764−12775

In this work, the total interaction energy (U_T) for a HP was considered as the sum of U_{vdW}, DL interaction energy (U_{DL}), and short-range repulsion. The short-range repulsion was evaluated by determining the Born potential energy (U_{BR}).[23] The DL and Born repulsion energies between the WHP or AHP and the solid collector surface are equal to those between the outer particle of the WHP or AHP and the surface (i.e., $U_{DL} = U_{DL}^{out}$ and $U_{BR} = U_{BR}^{out}$).[18] Therefore, the expressions used to calculate the total interaction energies for WHP and AHP are written as

$$U_T = U_{vdW}^{out} - U_{vdW}^{in} + U_{DL}^{out} + U_{BR}^{out} = U_T^{out} - U_{vdW}^{in} \text{ (for WHP)} \quad (7)$$

$$U_T = U_{vdW}^{out} - U_{vdW}^{in} + U_{WW}^{in} - U_{WC}^{in} + U_{DL}^{out} + U_{BR}^{out} = U_T^{out} - U_{vdW}^{in} + U_{WW}^{in} - U_{WC}^{in} \text{ (for AHP)} \quad (8)$$

It is worthwhile mentioning that the expressions used to calculate U_{vdW}^{in}, U_{WW}^{in}, and U_{WC}^{in} all have the form of $-A_{PWC}f(H)$, $-A_{WW}f(H)$, and $-A_{WC}f(H)$, respectively, where $f(H)$ is a function determined only by the geometrical data for an interaction configuration (e.g., size and shape of the particle, separation distance H between the particle and the collector). A_{PWC}, A_{WW}, and A_{WC} are Hamaker constants for particle−water−collector, water−water, and water−collector systems, respectively.

The eqs 4, 5, 7, and 8 are general expressions developed without using specific assumptions about the functional form of the vdW energy for WHPs and AHPs. The equations present expressions for calculating the vdW energies for HPs with different fillings by using the Hamaker approach. Alternatively, the Lifshitz approach[24] can be used to calculate the vdW interactions. In the Lifshitz approach, the Hamaker constant is derived in terms of bulk properties such as their dielectric constants and refractive indices.[7] Hamaker or Lifshitz approaches should provide similar results. For example, the Lifshitz approach also predicts that the Hamaker constants for the HP with air and vacuum inside are similar because the dielectric properties of air and vacuum are similar.

The interaction energy components on the right side of eqs 4, 5, 7, and 8 for a given WHP or AHP with a collector surface can be determined using approaches such as Derjaguin approximation (DA), surface element integration (SEI), and grid surface integration (GSI) techniques.[25−27] In the following section, we will use the SEI technique to calculate the vdW energy for spherical and cylindrical WHPs and AHPs. Although the DA technique cannot accurately calculate the interaction energies for nanoparticles, the SEI technique has overcome the limitations of the DA technique and can give accurate estimation of the interaction energy between a planar surface and a particle of any size and shape.[25] The GSI technique is similar to the SEI technique and can be used to calculate the interaction energy in the presence of surface charge heterogeneity.[27]

Calculation of Total Interaction Energy for Spherical and Cylindrical WHPs and AHPs. Interaction of a spherical or cylindrical WHP or AHP with a planar surface is schematically illustrated in Figure 1. For the interaction of a cylindrical HP with a planar surface, various orientations are possible. We only considered that the cylindrical HPs were oriented parallel or perpendicular to the planar surface (i.e., side-on or end-on orientations, respectively). Cylindrical HPs

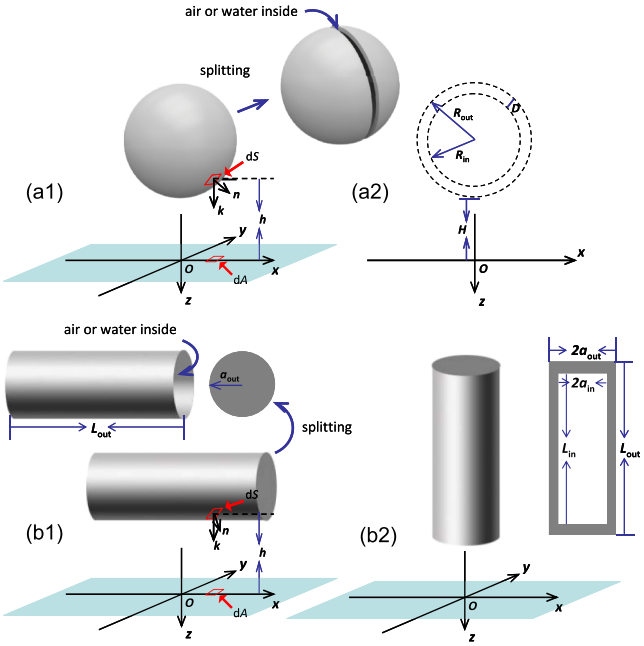

Figure 1. Coordinate systems used to describe (a) spherical or (b) cylindrical HP interacting with a planar surface. Part (a2) is a front view image of part (a1). Parts (b1) and (b2) show two different configurations of the cylindrical particle with the planar surface. R_{out} and R_{in} are the radii of the outer and inner spheres of the spherical HP, respectively, D is the shell thickness of the spherical HP, L_{out} and L_{in} are the outer and inner lengths of the cylindrical HP, respectively, a_{out} and a_{in} are the outer and inner radii of the cylindrical HP, respectively, dS is a differential area element on the HP surface, **k** is the unit vector directed toward the positive z axis, **n** is the outward unit normal to the particle surface, dA is the projected area of dS on the planar surface, h is the distance between dS and dA, and H is the separation distance between the HP and the planar surface.

can stably attach on a planar surface in two limiting orientations in the presence of flow. Stable attachment may occur for other orientations if aggregation or deformation occurs. However, we did not consider the aggregation and deformation of the cylindrical HPs. The Cartesian coordinate system was employed for the aforementioned interaction configurations. The xy plane of the coordinate system was oriented superposing the flat surface. The z-axis passes through the spherical HP center or superposes the central line of the cylindrical HP for the end-on orientation. The xz plane passes through the central line of the cylindrical HP, and the yz plane bisects the cylindrical HP into two equal segments for the side-on orientation. The outer surfaces of the spherical and cylindrical HPs were discretized into small area elements (dS).

The value of U_T^{out} for a spherical HP can be calculated using the following equation[18,25]

$$U_T^{out}(H) = \sum_S E_T(h)\mathbf{n}\cdot\mathbf{k}\, dS = \sum_A \left(E_T\left(H + R_{out} - \sqrt{{R_{out}}^2 - (x^2 + y^2)}\right) - E_T\left(H + R_{out} + \sqrt{{R_{out}}^2 - (x^2 + y^2)}\right)\right) dA \quad (9)$$

where E_T is the differential interaction energy between an area element dS on the outer surface of the spherical HP and the planar surface, H is the separation distance between the HP and the planar surface, h is the local separation distance

DOI: 10.1021/acs.langmuir.8b02547
Langmuir 2018, 34, 12764−12775

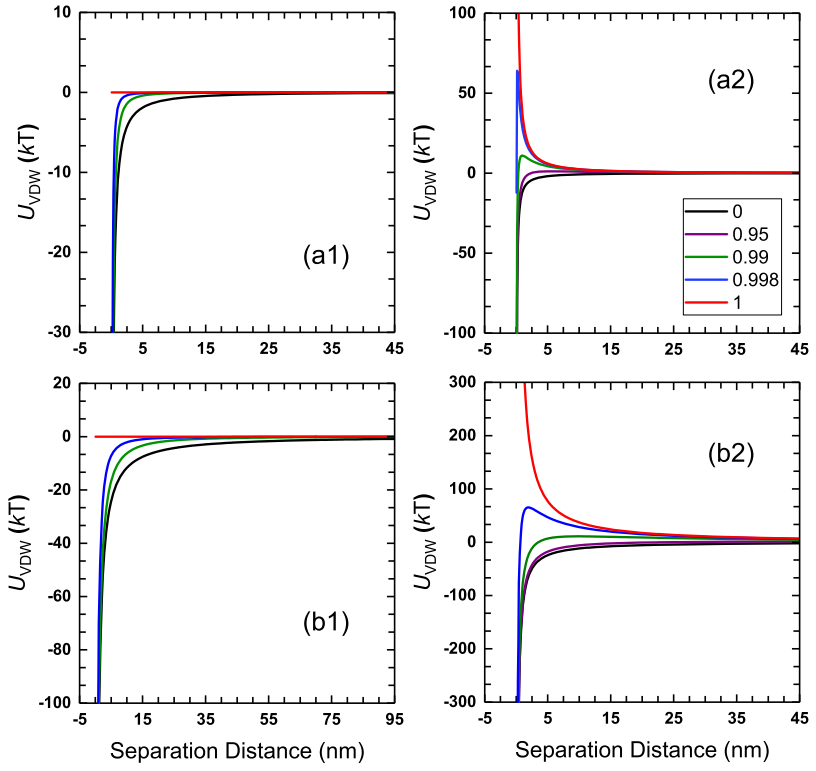

Figure 2. vdW energy profiles for a planar surface interacting with a (a) 100 or (b) 1000 nm spherical silica (1) WHP or (2) AHP of different ratios of R_{in} to R_{out}. R_{in}/R_{out} = 0 represents SPs. The spherical AHP becomes a spherical air bubble, and the WHP disappears for R_{in}/R_{out} = 1. Note the change in the scale of the *x*- and *y*-axes among the various graphs.

between the element dS and the planar surface, **n** is a unit vector outward normal to the outer surface of the spherical HP, **k** is a unit vector along the positive z-direction, S is the total surface area of the outer surface of the spherical HP, A is the total projected area of the outer surface of the spherical HP on the planar surface, R_{out} is the outer radius of the spherical HP, and dA is the projected area of dS on the planar surface.

The expressions used to calculate U_T^{out} for the cylindrical HP are

$$U_T^{out}(H) = \sum_A (E_T(H + a_{out} - \sqrt{a_{out}^2 - y^2}) - E_T(H + a_{out} + \sqrt{a_{out}^2 - y^2}))\, dA \quad \text{(side-on orientation)} \tag{10}$$

$$U_T^{out}(H) = (E_T(H) - E_T(H + L_{out}))S_{out}^{end} \quad \text{(end-on orientation)} \tag{11}$$

where a_{out} is the outer radius of the cylindrical HP, L_{out} is the outer length of the cylindrical HP, and S_{out}^{end} is the area of the top or bottom surface of the outer particle of the cylindrical HP.

The differential interaction energy E_T was calculated by adding E_{vdW}, E_{DL}, and E_{BR}. The following expressions were used to calculate E_{vdW}, E_{DL}, and E_{BR}[18,28,29]

$$E_{vdW}(h) = -\frac{A_{PWC}}{12\pi h^2} \tag{12}$$

$$E_{DL}(h) = \frac{\varepsilon\varepsilon_0\kappa}{2}\left[(\psi_p^2 + \psi_c^2)(1 - \coth \kappa h) + \frac{2\psi_p\psi_c}{\sinh \kappa h}\right] \tag{13}$$

$$E_{BR}(h) = \frac{A_{PWC}H_0^6}{48\pi h^8} \tag{14}$$

where A_{PWC} is the combined Hamaker constant of the interacting media, ε_0 is the dielectric permittivity of vacuum, ε is the dielectric constant of water, κ is the inverse Debye screening length, ψ_p and ψ_c are the surface potentials of the outer HP and the planar surface, respectively, and H_0 is the minimum separation distance, taken as 0.158 nm.[17] Note that the constant surface potential (CSP) boundary condition was assumed in eq 13 for calculating the DL energy.

The procedure used to calculate the U_{vdW}^{in} is similar to that for calculating U_{vdW}^{out}, which is written as

$$U_{vdW}^{in}(H) = \sum_A (E_{vdW}(H + R_{out} - \sqrt{R_{in}^2 - (x^2 + y^2)}) - E_{vdW}(H + R_{out} + \sqrt{R_{in}^2 - (x^2 + y^2)}))\, dA \quad \text{(for spherical HP)} \tag{15}$$

$$U_{vdW}^{in}(H) = \sum_A (E_{vdW}(H + a_{out} - \sqrt{a_{in}^2 - y^2}) - E_{vdW}(H + a_{out} + \sqrt{a_{in}^2 - y^2}))\, dA \quad \text{(for side-on orientation)} \tag{16}$$

DOI: 10.1021/acs.langmuir.8b02547
Langmuir 2018, 34, 12764−12775

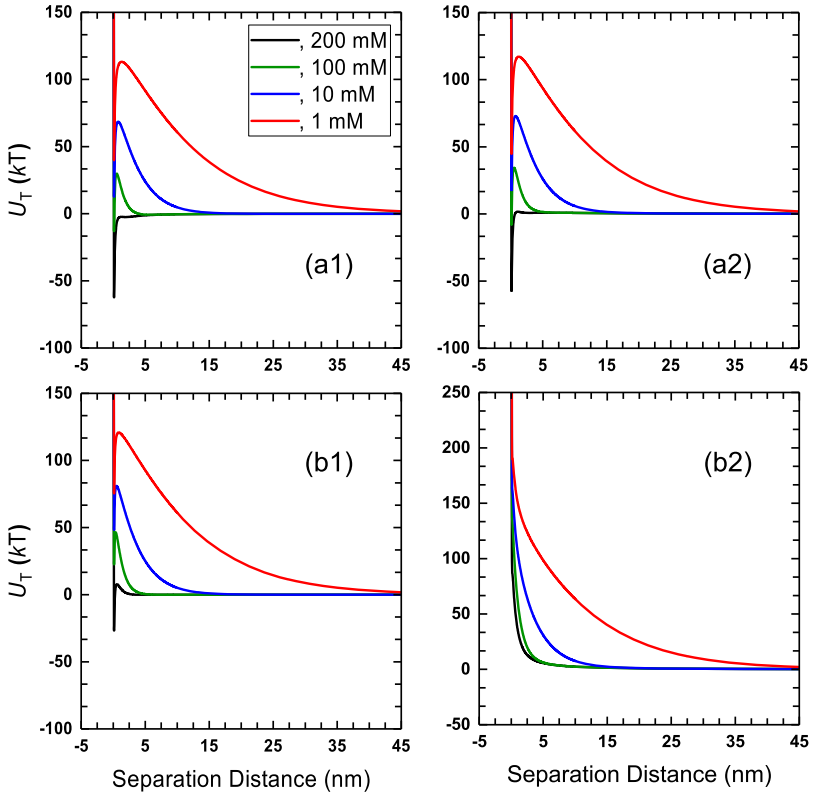

Figure 3. IEPs for a planar surface interacting with a 100 nm spherical silica (1) WHP or (2) AHP with values of R_{in}/R_{out} equal to 0.9 in (a) and 0.996 in (b) at different ISs. Note the change in the scale of the *x*- and *y*-axes among the various graphs.

$$U_{vdW}^{in}(H) = (E_{vdW}(H) - E_{vdW}(H + L_{in}))S_{in}^{end} \quad \text{(for end-on orientation)} \tag{17}$$

where R_{in} and a_{in} are the inner radii of the spherical and cylindrical HPs, respectively, L_{in} is the inner length of the cylindrical HP, S_{in}^{end} is the area of the top or bottom surface of the inner particle of the cylindrical HP, and A refers to the total projected area of the inner surface of the spherical or cylindrical HP on the planar surface. Equations 15−17 can also be used to calculate U_{WW}^{in} and U_{WC}^{in}; however, instead of using A_{PWC} to calculate E_{vdW}, we have to use A_{WW} and A_{WC} to calculate E_{vdW} for U_{WW}^{in} and $U_{WC}^{in}$of AHPs, respectively.

Unless otherwise specified, the shell compositions of the spherical HPs were assumed to be silica. Silica was adopted because it is one of the most widely used materials for fabricating spherical HPs.[30,31] Some results for carbon-based cylindrical HPs and spherical zero-valent iron (ZVI) HPs are given in the Supporting Information. The planar collector surface was assumed to have the same properties as those of a quartz surface. The DLVO interaction energies/forces between the spherical and cylindrical HPs and the planar surface were calculated at an ionic strength (IS) of 1, 10, 100, and 200 mM NaCl. DLVO energies are expressed in *kT*-units, where *k* is the Boltzmann constant and *T* is the absolute temperature taken as 293.15 K. The zeta potentials of silica HPs, CNTs, and quartz in NaCl at different IS were taken from Wang et al.[32,33] and Shen et al.[34] (see Table S1 of the Supporting Information). The zeta potentials of ZVI HPs were assumed to be zero. The measurement of Sun et al.[35] showed that the zeta potentials of ZVI particles decreased with increasing solution pH, which reached zero at about pH 8.2 (i.e., the isoelectric point). The values of the Hamaker constant for the water−water (A_{WW}), particle−water (A_{PW}), water−collector (A_{WC}), and particle−water−collector (A_{PWC}) systems are shown in Table S2 of the Supporting Information.

RESULTS AND DISCUSSION

vdW Energies between a HP and a Planar Surface. Figure 2 shows the vdW energy profiles for a planar surface interacting with a 100 or 1000 nm spherical silica SP and HPs (WHPs and AHPs) of different ratios of R_{in} to R_{out}. As expected, the value of U_{vdW} decreases monotonically (i.e., becomes more negative) with a decreasing separation distance for the SPs. The vdW energies for the WHPs are similar to those of SPs at very short separation distances (e.g., <1 nm) even if the shells of the WHPs are very thin. The result indicates that the value of U_{vdW} between a SP and a surface is primarily determined by a small fraction of the SP closest to the surface. At moderate separation distances (e.g., between 1 and 15 nm), increasing the value of R_{in}/R_{out} slightly increases the value of U_{vdW} for the WHPs. The aforementioned results explain why increasing the value of R_{in}/R_{out} has minor influence on the values of U_{pri} and U_{max} but can significantly reduce U_{sec} for a WHP, as have been shown in Shen et al.[18] The reduction of U_{sec} with an increasing value of R_{in}/R_{out} will be more significant if the retardation effect of vdW energy[36] at large separation distances is considered instead of using the nonretarded eq 12. However, as the trend for the variation of U_{sec} with R_{in}/R_{out} does not change, only eq 12 is used later in the paper for the calculation of vdW energy. When R_{in} is equal to R_{out}, the WHP disappears, and the water inside the WHP becomes a part of the bulk solution. In this case, the U_{vdW}^{out} is equal to U_{vdW}^{in} and the value of U_{vdW} in eq 4 becomes zero for the WHPs.

DOI: 10.1021/acs.langmuir.8b02547
Langmuir 2018, 34, 12764−12775

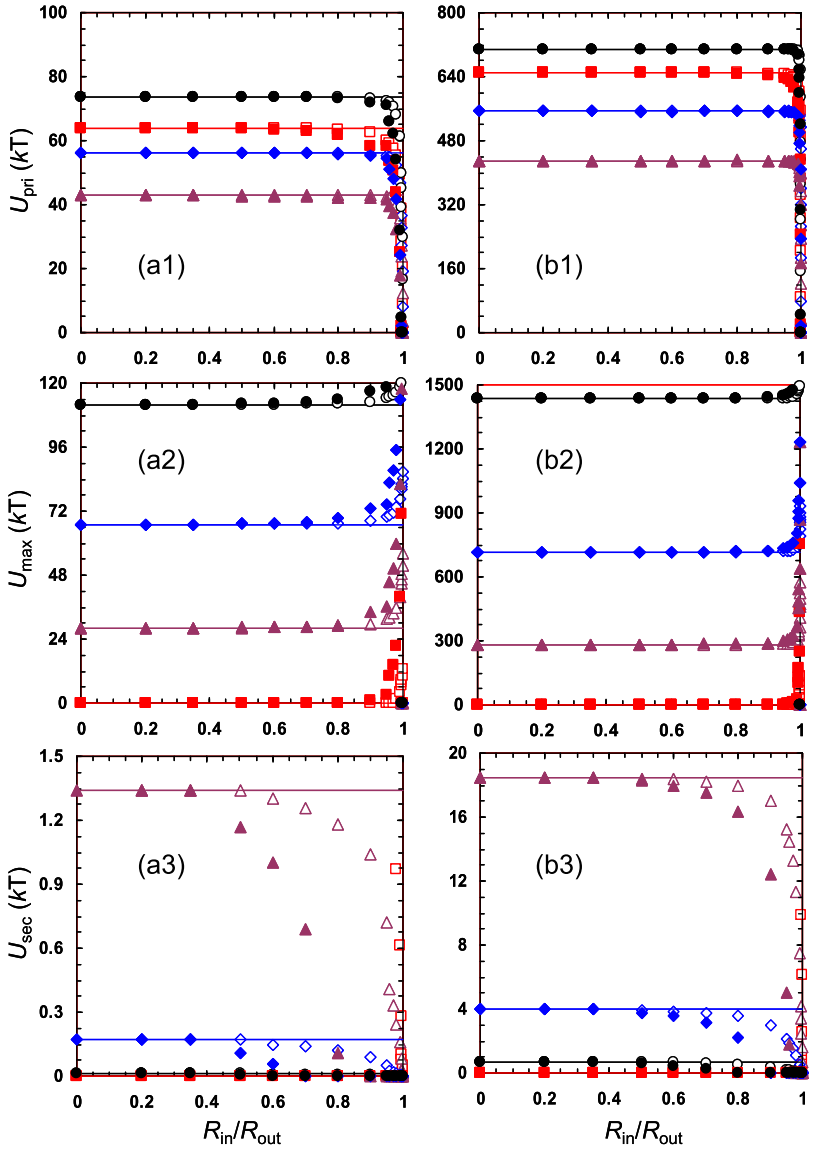

Figure 4. Calculated values of U_{pri}, U_{max}, and U_{sec} for a planar surface interacting with (a) 100 and (b) 1000 nm spherical silica WHPs (hollow symbols) or AHPs (solid symbols) with different inner radii under various IS conditions (spherical, 1 mM; diamond, 10 mM; triangle, 100 mM; square, 200 mM). The values of U_{pri}, U_{max}, and U_{sec} for the 100 and 1000 nm silica SPs (solid lines) are also shown.

Figure 2 shows that U_{vdW} is positive (i.e., repulsive) for the AHPs when the value of R_{in}/R_{out} is above a critical value. As shown in eq 5, the value of U_{vdW} for an AHP with a collector surface is equal to the sum of $U_{vdW}^{out} - U_{vdW}^{in}$ (i.e., vdW energy for a WHP) and $U_{WW}^{in} - U_{WC}^{in}$. The value of $U_{vdW}^{out} - U_{vdW}^{in}$ is negative and slightly decreases with increasing R_{in}/R_{out} until reaching zero at $R_{in} = R_{out}$ as shown above. The value of $U_{WW}^{in} - U_{WC}^{in}$, on the other hand, is positive and increases with increasing R_{in}/R_{out} (the maximum value is $U_{WW}^{out} - U_{WC}^{out}$). Therefore, at a critical value of R_{in}/R_{out}, the vdW energy for the AHP becomes zero. When the R_{in}/R_{out} of the AHP is above this critical value, the value of vdW energy for the HP becomes positive. For a given value of R_{in}/R_{out} above the critical ratio, there exists a critical separation distance where the value of U_{vdW} reaches a repulsive maximum, below and above which the value of U_{vdW} decreases until it reaches negative infinity (at a zero separation distance) and zero (when the separation distance is infinite), respectively. Such a nonmonotonic variation of U_{vdW} with a separation distance is due to the repulsive vdW energy between the air particle inside the AHP and the surface becomes more significant than the attractive vdW energy between the thin shell of the AHP and the surface at large separation distances, and the repulsive vdW energy of the air particle increases more rapidly with a decreasing separation distance compared to the attractive vdW energy of the AHP shell. However, the attractive vdW energy of the shell becomes dominant again at very small separation distances even if the shell is thin. At $R_{in}/R_{out} = 1$, the AHP becomes an air particle and the repulsive vdW energy between the air particle and planar surface increases monotonically with decreasing separation distance, and no attraction occurs at any separation distance. As the vdW energy is attractive at $R_{in}/R_{out} = 0$ and the vdW energy is repulsive at $R_{in}/R_{out} = 1$, there always exists a critical value of R_{in}/R_{out} between 0 and 1 at which the vdW energy is equal to zero for the AHP, irrespective of the specific value of the Hamaker constant used. However, the critical value of R_{in}/R_{out} increases with increasing the value of A_{PP}, as shown in Figure S1 of the

DOI: 10.1021/acs.langmuir.8b02547
Langmuir 2018, 34, 12764−12775

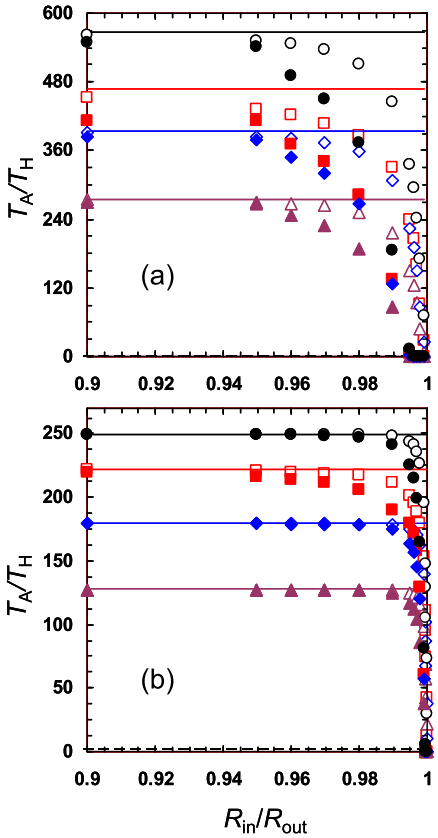

Figure 5. Calculated adhesive torque (T_A) normalized by a hydrodynamic drag torque (T_H) as a function of R_{in}/R_{out} for a planar surface interacting with the (a) 100 and (b) 1000 nm spherical silica WHPs (hollow symbols) and AHPs (solid symbols) under various IS conditions (spherical, 1 mM; diamond, 10 mM; triangle, 100 mM; square, 200 mM). Soil lines represent values of T_A/T_H for the 100 and 1000 nm spherical silica SPs and dashed line represents $T_A/T_H = 1$.

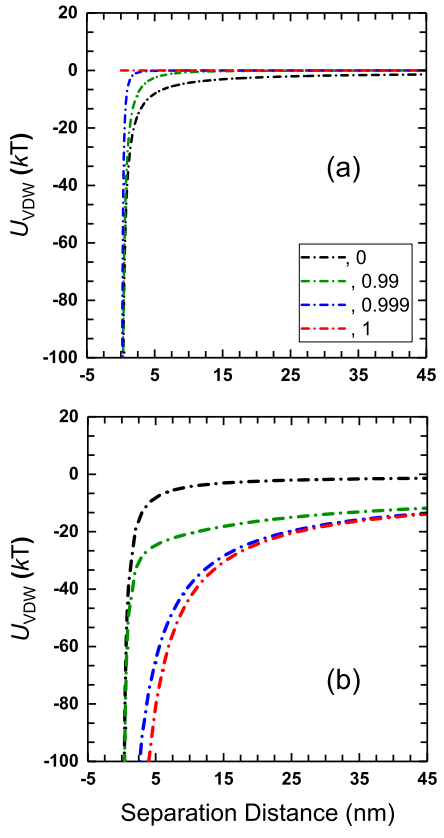

Figure 6. vdW energy profiles between two 1000 nm spherical silica (a) AHPs or (b) WHPs of different ratios of R_{in} to R_{out}. $R_{in}/R_{out} = 0$ represents SPs. The AHP becomes a spherical air bubble, and the WHP disappears for $R_{in}/R_{out} = 1$. Note the change in the scale of the *x*- and *y*-axes between the two graphs.

Supporting Information. Figure S2 shows similar trends for the variation of U_{vdW} with R_{in}/R_{out} and a separation distance for the cylindrical WHPs and AHPs by using the Hamaker constant of carbon for the calculations.

Total Interaction Energies between a HP and a Planar Surface. Figure 3 presents total DLVO interaction energy profiles (IEPs) between a planar surface and a 100 nm spherical silica AHP or WHP with R_{in}/R_{out} equal to 0.9 or 0.996 at different solution ISs. The IEPs for the WHP at $R_{in}/R_{out} = 0.9$ are similar to those of the 100 nm spherical silica SP shown in Figure S3 of the Supporting Information. Specifically, the IEPs of the WHP and SP are characterized by a deep primary minimum at a small separation distance, a maximum energy barrier, and a shallow secondary minimum at a larger distance (denoted as type I IEP) at IS ≤ 100 mM. The shallow secondary minima in the IEPs are highlighted in Figure S4 of the Supporting Information. At 200 mM, both the energy barrier and the secondary minimum disappear, and only the primary minimum exists in the IEPs of the WHP and SP (type II). The two types of IEPs have been widely reported in the literature.[37−39] When the value of R_{in}/R_{out} is increased to 0.996, the IEP changes from type II to type I because of the increase of the interaction energy barrier at 200 mM for the WHP.

For the AHP, two different types of IEPs are present. At $R_{in}/R_{out} = 0.9$, the secondary minimum disappears, and only primary minimum and maximum energy barrier are present in the IEP (type III) at IS ≤ 100 mM (Figure 3b1). At $R_{in}/R_{out} = 0.996$, the interaction energy decreases monotonically with increasing separation distance (type IV) at all solution ISs, indicating that the AHP experiences repulsive forces at all separation distances (Figure 3b2). Obviously, the interaction energy also decreases monotonically with an increasing separation distance for the air particle (i.e., $R_{in}/R_{out} = 1$) because of the existence of repulsive vdW energy at all separation distances. Such a monotonic decrease of interaction energy with an increasing separation distance will always occur for the AHPs when their shells are thin enough, irrespective of the Hamaker constants of the shell materials. The AHP cannot be attached on the surface in this case because of the repulsive forces and absence of energy minima. The type IV IEP has been shown to be present for SPs only when nanoscale surface roughness (NSR) is present.[39,40]

Figure 4 presents the calculated values of U_{pri}, U_{max}, and U_{sec} for 100 and 1000 nm SPs and spherical silica HPs (i.e., AHPs and WHPs) with different values of R_{in}/R_{out} at different solution ISs. The values of U_{pri} and U_{max} for the 100 nm HPs at $R_{in}/R_{out} \le 0.8$ and for the 1000 nm HPs at $R_{in}/R_{out} \le 0.9$ are similar to those of SPs. For the 100 nm HP at $R_{in}/R_{out} > 0.8$ and the 1000 nm HP at $R_{in}/R_{out} > 0.9$, the values of U_{pri} and U_{max} decrease and increase with increasing R_{in}/R_{out}, respectively. The trend for the variation of U_{sec} with R_{in}/R_{out} is similar to that of U_{pri} with R_{in}/R_{out} for the 100 and 1000 nm HPs. However, the critical values of R_{in}/R_{out} at which the U_{sec}

DOI: 10.1021/acs.langmuir.8b02547
Langmuir 2018, 34, 12764−12775

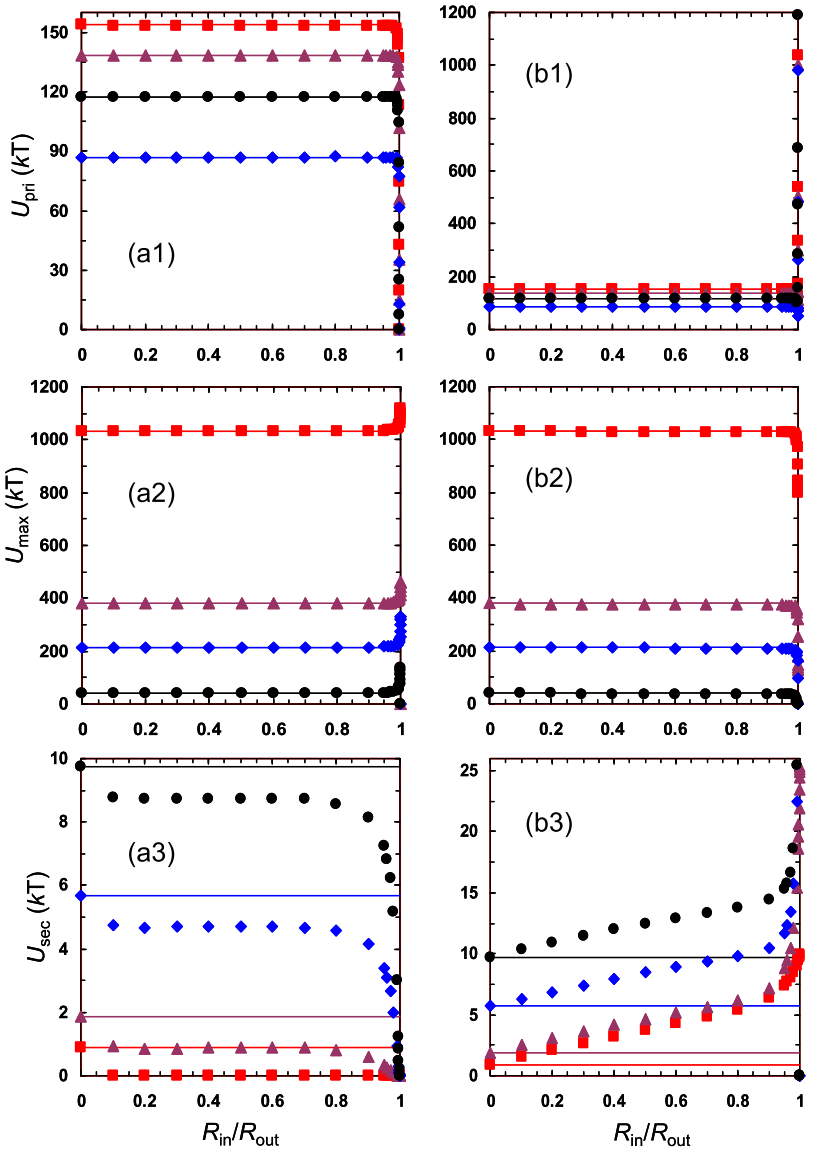

Figure 7. Calculated values of U_{pri}, U_{max}, and U_{sec} between two 1000 nm spherical silica (a) WHPs or (b) AHPs with different ratios of R_{in} to R_{out} under various IS conditions (spherical, 200 mM; diamond, 100 mM; triangle, 10 mM; square, 1 mM). The values of U_{pri}, U_{max}, and U_{sec} between two 1000 nm silica SPs (solid lines) were also shown.

begins to decrease (0.4 and 0.5 for the 100 and 1000 nm HPs, respectively) are smaller than those for the U_{pri}. The decrease of U_{pri} and U_{sec} and the increase of U_{max} with increasing R_{in}/R_{out} are more rapid for the AHPs than for the WHPs because of more significant increase of vdW energy (i.e., less attractive or even repulsive) for the AHPs. These results indicate that the attachment in primary and secondary minima is inhibited when the shell thicknesses of the HPs are small, especially for spherical AHPs. Similarly, the cylindrical AHPs are also less readily attached in the primary and secondary minima compared to the cylindrical WHPs for both side-on and end-on orientations (cf., Figure S5 of the Supporting Information). In particular, both primary and secondary minima disappear, and the attachment cannot occur at all considered ISs when the shells of the cylindrical AHPs are thin (e.g., $R_{in}/R_{out} > 0.99$). Notably, the results of Figures 4 and S5 were obtained by assuming the CSP boundary condition for calculating the DL interaction energy; yet, the trend for the variation of U_{pri}, U_{max}, and U_{sec} with R_{in}/R_{out} for the WHPs and AHPs does not change if linearized superposition approximation (LSA)[41] approach was adopted for the DL energy calculations (see Figure S6 in the Supporting Information). Therefore, only the CSP condition is used for calculating the DL energies later in the paper. However, for a given value of R_{in}/R_{out}, the primary and secondary minimum attachments are reduced for the WHPs and AHPs under the LSA condition compared to those under the CSP condition. This is because the DL interaction energy is more repulsive under the LSA condition than the CSP condition. Although the constant surface charge (CSC) approach has also been used for determining the DL energy, this boundary condition requires that the potentials of interacting surfaces tend to reach infinity as they approach each other.[42] Therefore, the CSC approach cannot accurately determine the DL energies at small separation distances.[43]

Our results are qualitatively consistent with Lifshitz theory, which predicts repulsive vdW interactions between air and silica.[44] The results are also consistent with experimental observations of complete breakthrough (i.e., no attachment)

DOI: 10.1021/acs.langmuir.8b02547
Langmuir 2018, 34, 12764−12775

for the transport of bubbles through quartz sand media[22] and insignificant attachment of single-walled CNTs during transport in porous media.[2,9,45] The attachment of CNTs in porous media was not completely inhibited[2,9] likely because the single-walled CNTs were WHPs rather than AHPs because of the possible imbibition of water into the CNTs. The attachment of CNTs would be further reduced if caps are used to close the ends of the cylindrical, single-walled CNT,[46] which would prevent the imbibition of water. In addition, the presence of physical and chemical heterogeneities on soil surfaces can cause attractive DL energy between the CNTs and surfaces, which could exceed the repulsive vdW energy and thus increase the attachment.[47] Possible deformation of single-walled CNTs may also increase the attachment. For multi-walled CNTs, the energy wells and attachment are more significant than single-walled CNTs because of an increase of the shell thickness.[48−51]

A reduction of attachment and an increase of detachment for HPs occur when U_{pri} becomes similar in magnitude to the average kinetic energy of a colloid (1.5 kT). In this case, HPs can readily escape from shallow primary energy wells by Brownian diffusion. Moreover, if flow is present, a HP also cannot attach in a primary minimum when the adhesive torque is smaller than the applied hydrodynamic torque.[52,53] Figure 5 compares adhesive torques (T_A) for 100 and 1000 nm spherical silica WHPs and AHPs of various shell thicknesses at different ISs when a hydrodynamic drag torque (T_H) is applied that is typical for a groundwater flow velocity of 7 m/d in a coarse textured porous medium.[54] Details for the calculation of T_A and T_H are shown in the Supporting Information. Figure 5 shows that the trend for the variation of T_A with R_{in}/R_{out} is similar to that of U_{pri} with R_{in}/R_{out} in Figure 4 because the primary minimum depth determines both the adhesive force and torque on a smooth surface.[7] Specifically, the value of T_A decreases with increasing R_{in}/R_{out} above a critical value for the WHPs and AHPs. However, the value of T_A is still larger than T_H for the WHPs even if the value of R_{in}/R_{out} is close to 1. In contrast, the value of T_A becomes smaller than T_H when the value of R_{in}/R_{out} is larger than 0.99 and 0.999 for the 100 and 1000 nm AHPs, respectively. Therefore, the silica AHPs cannot be attached in these cases. The range of R_{in}/R_{out} at which $T_A/T_H \leq 1$ will be much larger for the AHPs if NSR is present on the collector surface because the NSR can significantly reduce the primary minimum depth and accordingly the adhesive force and torque.[55−57]

The fabrication of nanomaterials with the AHP structure could potentially be exploited for soil remediation because their reduced or even repulsive vdW energy inhibits attachment in primary and secondary minima. For example, although ZVI SPs have been shown to be very effective for the treatment of a variety of pollutants,[58] the use of ZVI SPs for in situ remediation of contaminated soil is limited because of their very low mobility in the soil.[59,60] The low mobility of ZVI in soil occurs because the absence of an energy barrier between ZVI SPs and negatively charged soil grain surfaces produces favorable attachment conditions. However, if a ZVI particle is hollow and air filled, then an energy barrier appears for spherical ZVI AHPs with small shell thickness and attachment changes from favorable to unfavorable (see Figure S7). The presence of the energy barrier is solely due to the repulsive vdW energy as the DL energy is attractive for ZVI particles by assuming zero zeta potentials for the ZVI particles and using the CSP condition for calculations. No secondary minimum exists for all shell thicknesses because of the attractive DL energy. The secondary minimum is present because the vdW attraction decreases more slowly with an increasing separation distance than the repulsive DL energy.[37,38] The primary minima also disappear and attachment cannot occur when the shells of ZVI AHPs are thin. Figure S8 shows that the values of U_{max} can be larger than 500 kT for interaction between the 1000 nm ZVI AHPs with thin shells and a planar surface. These large energy barriers can prevent the ZVI AHP from being attached at primary minima.[55] In contrast, no energy barrier exists for the 1000 nm ZVI WHP and favorable attachment will occur at all values of R_{in}/R_{out}. The ZVI AHPs with thin shells therefore show a greater potential for in situ remediation of contaminated soil than ZVI WHPs because the presence of repulsive energy barrier produces greater mobility in subsurface environments. In addition, AHPs with thin shells experience much lower sedimentation in solution compared to SPs and WHPs, and this will further enhance their mobility.

Note that the ZVI surface is readily oxidized in the environment, which will increase the attractive DL energy because the isoelectric points of iron oxides are larger than that of ZVI. Accordingly, the mobility of oxidized ZVI AHPs will be decreased. However, the oxidized ZVI particles are readily coated with natural organic matter, which is ubiquitous in subsurface environments.[61] This coating can cause negative zeta potentials for the ZVI AHPs even if the solution pH is below the isoelectric point.[62−64] The coated ZVI AHPs will have great mobility as both vdW and DL energies are repulsive and the steric repulsion is present.

Total Interaction Energies between Two HPs. Figure 6 presents the vdW energy profiles between two 1000 nm spherical silica AHPs or WHPs of different values of R_{in}/R_{out}. Detailed methods used to calculate the vdW interaction energies between two AHPs and WHPs have been shown in the Supporting Information. The trend for the variation of vdW energy between the two WHPs with R_{in}/R_{out} is similar to that between a WHP and a planar surface. In particular, the vdW energies between the two silica WHPs are similar to those between the two corresponding SPs at very short separation distances (e.g., <1 nm) because the vdW energy is mainly determined by a small fraction of WHPs or SPs when the two WHPs or SPs are close to each other. At moderate separation distances (e.g., between 1 and 25 nm), the vdW interaction energies become less negative when the value of R_{in}/R_{out} increases. When the R_{in} is equal to R_{out}, the two WHPs disappear and the water inside the WHPs becomes part of the bulk solution. In this case, the value of U_{vdW} is equal to zero [see eq S6 of the Supporting Information].

Recall that the vdW energy between an AHP and a planar surface becomes less attractive with increasing R_{in}/R_{out} and can even become repulsive when the R_{in}/R_{out} is above a critical value (e.g., Figure 2). In contrast to the interaction of an AHP and a planar surface, the vdW energy becomes more negative, that is, more attractive, with increasing R_{in}/R_{out} between the two AHPs (Figure 6). The two AHPs become air particles when $R_{in}/R_{out} = 1$, and the value of U_{vdW} reaches a minimum that is equal to U_{WW}^{AA} (the vdW energy between two water particles with sizes equal to the two AHPs in vacuum, see eq S7). The aggregation of air particles ($R_{in}/R_{out} = 1$) is more favorable than that of SPs in water because of increased vdW attraction, which explains why bubble aggregation in liquid is a favorable process.[65,66] The favorable aggregation of air particles is more significant if the sizes of the air particles are larger

DOI: 10.1021/acs.langmuir.8b02547
Langmuir 2018, 34, 12764−12775

because the value of U_{WW}^{AA} is more negative for interaction between larger particles, which is in agreement with the experimental observation that aggregation is more significant for microbubbles than nanobubbles.[67] Although the important role of vdW interactions for bubble interaction has been experimentally recognized recently,[68] our study provides expression to exactly evaluate the vdW energy between bubbles. Once the bubbles contact each other, the bubble coalescence will be driven by the reduction of surface energy.[69]

Figure 7 shows the calculated values of U_{pri}, U_{max}, and U_{sec} between two 1000 nm spherical silica WHPs or AHPs as a function of R_{in}/R_{out} under various IS conditions. The values of U_{pri}, U_{max}, and U_{sec} between the two WHPs or AHPs are similar to those between the two corresponding SPs when the value of R_{in}/R_{out} is small. However, when R_{in}/R_{out} is above a critical value, U_{pri} and U_{sec} decrease and U_{max} increases with R_{in}/R_{out} between the two WHPs because of a reduction of vdW attraction. Hence, the aggregation in the primary and secondary minima with a larger value of R_{in}/R_{out} is less likely for the two WHPs. For the interaction between the two AHPs, the value of U_{sec} increases with increasing R_{in}/R_{out} because of an increase of vdW attraction. The value of U_{sec} can be increased to be larger than 10 kTs even at the lowest IS used (i.e., 1 mM). Bradford et al.[54] demonstrated that an energy depth of 7 kT can essentially prevent colloid detachment by Brownian diffusion. Therefore, the aggregation in a secondary minimum is more favored for AHPs compared to SPs and WHPs. In addition, the value of U_{max} between the two AHPs decreases with increasing R_{in}/R_{out} above a critical value and can even disappear at IS $\geq$ 100 mM when the shells of the AHP are thin. Accordingly, the 1000 nm AHPs are favored to be aggregated in a primary minimum in these cases. These results can explain why AHPs readily aggregate in solutions and reagents, and why perturbations have to be applied to disperse them.[3,70] The aggregation of AHPs will be further enhanced when short-range attractions (e.g., hydrophobic interactions for closed-cap CNTs) exist between the AHPs. The aggregated AHPs still have low affinity to attach on collector surfaces because the interaction of an aggregate with a surface is mainly controlled by those of the primary particles of the aggregate with the surface.[71]

Figure S9 shows the calculated values of U_{pri}, U_{max}, and U_{sec} between two spherical silica AHPs with different values of R_{out} under various IS conditions. The shell thickness of the AHPs was fixed to be 0.25 nm. The results indicate that microsized AHPs are more likely to aggregate than nanosized AHPs. Specifically, only a primary minimum is present for all values of R_{out} when IS = 200 mM, and the value of U_{pri} increases with increasing R_{out}. Hence, the aggregation of microsized AHPs is more favorable than for nanosized AHPs. At IS $\leq$ 100 mM, the value of U_{sec} increases with increasing R_{out}. The values of U_{sec} are larger than 10 kT at all ISs considered for microsized AHPs. Microsized AHPs are therefore more likely to be aggregated in a secondary minimum compared to nanosized AHPs when IS $\leq$ 100 mM.

SUMMARY AND CONCLUSIONS

We demonstrated that the subtraction method used in the literature to calculate the vdW energy between a HP and a surface is only valid for WHPs and present general expressions to calculate the vdW energy between an AHP and a planar surface and between two AHPs. The calculations show that although only attachment in secondary minima is reduced for the WHPs compared to SPs, both attachments in primary and secondary minima are inhibited for AHPs when their shells are thin. A repulsive energy barrier can even exist between an AHP and a negatively charged planar surface because of the repulsive vdW energy, changing the attachment from favorable to unfavorable. Although aggregation in primary and secondary minima is reduced for HPs compared to SPs, the aggregation in primary and secondary minima is enhanced between AHPs when their shells are thin and thick, respectively.

These findings have important implications for various applications of HP in porous media. For instance, ZVI, a potent nanoparticle used for groundwater remediation, usually shows limited mobility in subsurface media, thereby limiting its applicability. A ZVI HP with air and a thin iron shell, however, would show repulsive interactions with a typical subsurface collector (i.e., quartz) and thus would be much more mobile than the traditional ZVI SPs.

ASSOCIATED CONTENT

Supporting Information

The Supporting Information is available free of charge on the ACS Publications website at DOI: 10.1021/acs.langmuir.8b02547.

Methods for calculating adhesive and hydrodynamic torques, interaction energies between two WHPs and AHPs, and interaction energies between a HP and a planar surface, zeta potentials of colloids and quartz, values of Hamaker constants for various materials, calculated critical value of R_{in}/R_{out} as a function of the value of A_{pp} for different values of R_{out}, vdW energy profiles for a planar surface interacting with a cylindrical carbon AHP or WHP in side-on or end-on orientations, IEPs for a planar surface interacting with a 100 nm spherical silica SP under various IS conditions and interacting with 100 nm spherical ZVI AHPs and WHPs, replotted IEPs in Figure 3 to highlight the depth and location of secondary minima, calculated values of U_{pri}, U_{max}, and U_{sec} for cylindrical carbon WHPs and AHPs in side-on and end-on orientations, for a 1000 nm spherical silica WHP and AHP interacting with a planar surface by using the LSA condition for DL energy calculations, for a 1000 nm spherical ZVI WHP and AHP, and between two spherical silica AHPs at different values of R_{out} with a shell thickness of 0.25 nm (PDF)

AUTHOR INFORMATION

Corresponding Authors

*E-mail: Scott.Bradford@ars.usda.gov. Phone: (951) 369-4857. Fax: (951) 342-4964 (S.B.).

*E-mail: libg@cau.edu.cn. Phone: +86 1062732850. Fax: +86 1062733596 (B.L.).

ORCID

Chongyang Shen: 0000-0002-2517-3472

Scott A. Bradford: 0000-0002-3260-2968

Markus Flury: 0000-0002-3344-3962

Notes

The authors declare no competing financial interest.

ACKNOWLEDGMENTS

C.S. acknowledges the funding by the National Natural Science Foundation of China (41671222 and 41271009), the National

DOI: 10.1021/acs.langmuir.8b02547
Langmuir 2018, 34, 12764−12775

Key Research and Development Program of China (2017YFD0800301), and the Beijing Nova Program (Z161100004916116). M.F. was in part supported by the National Institute of Food and Agriculture Hatch Project 1014527.

REFERENCES

(1) Wang, X.; Feng, J.; Bai, Y.; Zhang, Q.; Yin, Y. Synthesis, properties, and applications of hollow micro-/nanostructures. *Chem. Rev.* **2016**, *116*, 10983−11060.
(2) Jaisi, D. P.; Saleh, N. B.; Blake, R. E.; Elimelech, M. Transport of single-walled carbon nanotubes in porous media: Filtration mechanisms and reversibility. *Environ. Sci. Technol.* **2008**, *42*, 8317−8323.
(3) Bouchard, D.; Zhang, W.; Powell, T.; Rattanaudompol, U.-s. Aggregation kinetics and transport of single-walled carbon nanotubes at low surfactant concentrations. *Environ. Sci. Technol.* **2012**, *46*, 4458−4465.
(4) De Volder, M. F. L.; Tawfick, S. H.; Baughman, R. H.; Hart, A. J. Carbon Nanotubes: Present and Future Commercial Applications. *Science* **2013**, *339*, 535−539.
(5) Caruso, F.; Caruso, R. A.; Möhwald, H. Nanoengineering of inorganic and hybrid hollow spheres by colloidal templating. *Science* **1998**, *282*, 1111−1114.
(6) Hu, J.; Chen, M.; Fang, X.; Wu, L. Fabrication and application of inorganic hollow spheres. *Chem. Soc. Rev.* **2011**, *40*, 5472−5491.
(7) Israelachvili, J. N. *Intermolecular and Surface Forces*, 3rd ed.; Academic Press: Waltham, 2011.
(8) Wu, L.; Gao, B.; Tian, Y.; Muñoz-Carpena, R.; Zigler, K. J. DLVO interactions of carbon nanotubes with isotropic planar surfaces. *Langmuir* **2013**, *29*, 3976−3988.
(9) Jaisi, D. P.; Elimelech, M. Single-walled carbon nanotubes exhibit limited transport in soil columns. *Environ. Sci. Technol.* **2009**, *43*, 9161−9166.
(10) Peng, X.; Li, Y.; Luan, Z.; Di, Z.; Wang, H.; Tian, B.; Jia, Z. Adsorption of 1,2-dichlorobenzene from water to carbon nanotubes. *Chem. Phys. Lett.* **2003**, *376*, 154−158.
(11) Zhang, Y.; Xu, S.; Luo, Y.; Pan, S.; Ding, H.; Li, G. Synthesis of mesoporous carbon capsules encapsulated with magnetite nanoparticles and their application in wastewater treatment. *J. Mater. Chem.* **2011**, *21*, 3664−3671.
(12) Kretzschmar, R.; Borkovec, M.; Grolimund, D.; Elimelech, M. Mobile subsurface colloids and their role in contaminant transport. *Adv. Agron.* **1999**, *66*, 121−193.
(13) de Jonge, L. W.; Kjaergaard, C.; Moldrup, P. Colloids and Colloid-Facilitated Transport of Contaminants in Soils. *Vadose Zone J.* **2004**, *3*, 321−325.
(14) Sen, T. K.; Khilar, K. C. Review on subsurface colloids and colloid-associated contaminant transport in saturated porous media. *Adv. Colloid Interface Sci.* **2006**, *119*, 71−96.
(15) Ryan, J. N.; Elimelech, M. Colloid mobilization and transport in groundwater. *Colloids Surf., A* **1996**, *107*, 1−56.
(16) Verwey, E. J. W.; Overbeek, J. T. G. *Theory of the Stability of Lyophobic Colloids*; Elsevier: New York, 1948.
(17) Hoek, E. M. V.; Agarwal, G. K. Extended DLVO interactions between spherical particles and rough surfaces. *J. Colloid Interface Sci.* **2006**, *298*, 50−58.
(18) Shen, C.; Bradford, S.; Wang, Z.; Huang, Y.; Zhang, Y.; Li, B. DLVO interaction energies between hollow spherical particles and collector surfaces. *Langmuir* **2017**, *33*, 10455−10467.
(19) Hamaker, H. C. The London-van der Waals attraction between spherical particles. *Physica* **1937**, *4*, 1058−1072.
(20) Kumar, A.; Gu, S. Modelling impingement of hollow metal droplets onto a flat surface. *Int. J. Heat Fluid Flow* **2012**, *37*, 189−195.
(21) Zhang, M.; Bradford, S. A.; Šimůnek, J.; Vereecken, H.; Klumpp, E. Do Goethite Surfaces Really Control the Transport and Retention of Multi-Walled Carbon Nanotubes in Chemically Heterogeneous Porous Media? *Environ. Sci. Technol.* **2016**, *50*, 12713−12721.
(22) Wan, J.; Veerapaneni, S.; Gadelle, F.; Tokunaga, T. K. Generation of stable microbubbles and their transport through porous media. *Water Resour. Res.* **2001**, *37*, 1173−1182.
(23) Ruckenstein, E.; Prieve, D. C. Adsorption and desorption of particles and their chromatographic separation. *AIChE J.* **1976**, *22*, 276−283.
(24) Lifshitz, E. M. The theory of molecular attractive forces between solids. *J. Exp. Theor. Phys.* **1956**, *2*, 73−83.
(25) Bhattacharjee, S.; Elimelech, M. Surface element integration: A novel technique for evaluation of DLVO interaction between a particle and a flat plate. *J. Colloid Interface Sci.* **1997**, *193*, 273−285.
(26) Bhattacharjee, S.; Ko, C.-H.; Elimelech, M. DLVO interaction between rough surfaces. *Langmuir* **1998**, *14*, 3365−3375.
(27) Duffadar, R. D.; Davis, J. M. Interaction of micrometer-scale particles with nanotextured surfaces in shear flow. *J. Colloid Interface Sci.* **2007**, *308*, 20−29.
(28) Hogg, R.; Healy, T. W.; Fuerstenau, D. W. Mutual coagulation of colloidal dispersions. *Trans. Faraday Soc.* **1966**, *62*, 1638−1651.
(29) Oliveira, R. Understanding adhesion: a means for preventing fouling. *Exp. Therm. Fluid Sci.* **1997**, *14*, 316−322.
(30) Dai, H. Carbon nanotubes: Synthesis, integration, and properties. *Acc. Chem. Res.* **2002**, *35*, 1035−1044.
(31) Eatemadi, A.; Daraee, H.; Karimkhanloo, H.; Kouhi, M.; Zarghami, N.; Akbarzadeh, A.; Abasi, M.; Hanifehpour, Y.; Joo, S. Carbon nanotubes: properties, synthesis, purification, and medical applications. *Nanoscale Res. Lett.* **2014**, *9*, 393.
(32) Wang, C.; Bobba, A. D.; Attinti, R.; Shen, C.; Lazouskaya, V.; Wang, L.-P.; Jin, Y. Retention and transport of silica nanoparticles in saturated porous media: Effect of concentration and particle size. *Environ. Sci. Technol.* **2012**, *46*, 7151−7158.
(33) Wang, H.; Huang, Y.; Shen, C.; Wu, J.; Yan, A.; Zhang, H. Co-transport of pesticide acetamiprid and silica nanoparticles in biochar-amended sand porous media. *J. Environ. Qual.* **2016**, *45*, 1749−1759.
(34) Shen, C.; Li, B.; Huang, Y.; Jin, Y. Kinetics of Coupled Primary- and Secondary-Minimum Deposition of Colloids under Unfavorable Chemical Conditions. *Environ. Sci. Technol.* **2007**, *41*, 6976−6982.
(35) Sun, Y.-P.; Li, X.-q.; Cao, J.; Zhang, W.-x.; Wang, H. P. Characterization of zero-valent iron nanoparticles. *Adv. Colloid Interface Sci.* **2006**, *120*, 47−56.
(36) Gregory, J. Approximate expressions for retarded van der waals interaction. *J. Colloid Interface Sci.* **1981**, *83*, 138−145.
(37) Hahn, M. W.; O'Melia, C. R. Deposition and reentrainment of Brownian particles in porous media under unfavorable chemical conditions: Some concepts and applications. *Environ. Sci. Technol.* **2004**, *38*, 210−220.
(38) Hahn, M. W.; Abadzic, D.; O'Melia, C. R. Aquasols: On the Role of Secondary Minima. *Environ. Sci. Technol.* **2004**, *38*, 5915−5924.
(39) Torkzaban, S.; Bradford, S. A. Critical role of surface roughness on colloid retention and release in porous media. *Water Res.* **2016**, *88*, 274−284.
(40) Shen, C.; Wang, F.; Li, B.; Jin, Y.; Wang, L.-P.; Huang, Y. Application of DLVO energy map to evaluate interactions between spherical colloids and rough surfaces. *Langmuir* **2012**, *28*, 14681−14692.
(41) Gregory, J. Interaction of unequal double layers at constant charge. *J. Colloid Interface Sci.* **1975**, *51*, 44−51.
(42) Adamczyk, Z.; Weroński, P. Application of the DLVO theory for particle deposition problems. *Adv. Colloid Interface Sci.* **1999**, *83*, 137−226.
(43) Shen, C.; Bradford, S. A.; Li, T.; Li, B.; Huang, Y. Can nanoscale surface charge heterogeneity really explain colloid detachment from primary minima upon reduction of solution ionic strength? *J. Nanopart. Res.* **2018**, *20*, 165.
(44) Hough, D. B.; White, L. R. The calculation of Hamaker constants from Liftshitz theory with applications to wetting phenomena. *Adv. Colloid Interface Sci.* **1980**, *14*, 3−41.
(45) Wang, Y.; Kim, J.-H.; Baek, J.-B.; Miller, G. W.; Pennell, K. D. Transport behavior of functionalized multi-wall carbon nanotubes in

DOI: 10.1021/acs.langmuir.8b02547
Langmuir 2018, 34, 12764−12775

water-saturated quartz and as a function of tube length. *Water Res.* **2012**, *46*, 4521−4531.
(46) de Jonge, N.; Doytcheva, M.; Allioux, M.; Kaiser, M.; Mentink, S. A. M.; Teo, K. B. K.; Lacerda, R. G.; Milne, W. I. Cap closing of thin carbon nanotubes. *Adv. Mater.* **2005**, *17*, 451−455.
(47) Hamamoto, S.; Takemura, T.; Suzuki, K.; Nishimura, T. Effects of pH on nano-bubble stability and transport in saturated porous media. *J. Contam. Hydrol.* **2018**, *208*, 61−67.
(48) Liu, X.; O'Carroll, D. M.; Petersen, E. J.; Huang, Q.; Anderson, C. L. Mobility of multiwalled carbon nanotubes in porous media. *Environ. Sci. Technol.* **2009**, *43*, 8153−8158.
(49) Tian, Y.; Gao, B.; Wu, L.; Muñoz-Carpena, R.; Huang, Q. Effect of solution chemistry on multi-walled carbon nanotube deposition and mobilization in clean porous media. *J. Hazard. Mater.* **2012**, *231−232*, 79−87.
(50) O'Carroll, D. M.; Liu, X.; Mattison, N. T.; Petersen, E. J. Impact of diameter on carbon nanotube transport in sand. *J. Colloid Interface Sci.* **2013**, *390*, 96−104.
(51) Han, B.; Liu, W.; Zhao, X.; Cai, Z.; Zhao, D. Transport of multi-walled carbon nanotubes stabilized by carboxymethyl cellulose and starch in saturated porous media: Influences of electrolyte, clay and humic acid. *Sci. Total Environ.* **2017**, *599-600*, 188−197.
(52) Bergendahl, J.; Grasso, D. Prediction of colloid detachment in a model porous media: hydrodynamics. *Chem. Eng. Sci.* **2000**, *55*, 1523−1532.
(53) Bergendahl, J. A.; Grasso, D. Mechanistic basis for particle detachment from granular media. *Environ. Sci. Technol.* **2003**, *37*, 2317−2322.
(54) Torkzaban, S.; Bradford, S. A.; Wan, J.; Tokunaga, T.; Masoudih, A. Release of quantum dot nanoparticles in porous media: Role of cation exchange and aging time. *Environ. Sci. Technol.* **2013**, *47*, 11528−11536.
(55) Bradford, S. A.; Kim, H.; Shen, C.; Sasidharan, S.; Shang, J. Contributions of nanoscale roughness to anomalous colloid retention and stability behavior. *Langmuir* **2017**, *33*, 10094−10105.
(56) Shen, C.; Jin, Y.; Li, B.; Zheng, W.; Huang, Y. Facilitated attachment of nanoparticles at primary minima by nanoscale roughness is susceptible to hydrodynamic drag under unfavorable chemical conditions. *Sci. Total Environ.* **2014**, *466−467*, 1094−1102.
(57) Rasmuson, A.; Pazmino, E.; Assemi, S.; Johnson, W. P. Contribution of nano- to microscale roughness to heterogeneity: Closing the gap between unfavorable and favorable colloid attachment conditions. *Environ. Sci. Technol.* **2017**, *51*, 2151−2160.
(58) Zhang, W.-X. Nanoscale iron particles for environmental remediation: An overview. *J. Nanopart. Res.* **2003**, *5*, 323−332.
(59) Johnson, R. L.; Nurmi, J. T.; O'Brien Johnson, G. S.; Fan, D.; O'Brien Johnson, R. L.; Shi, Z.; Salter-Blanc, A. J.; Tratnyek, P. G.; Lowry, G. V. Field-scale transport and transformation of carboxymethylcellulose-stabilized nano zero-valent iron. *Environ. Sci. Technol.* **2013**, *47*, 1573−1580.
(60) Kocur, C. M.; Chowdhury, A. I.; Sakulchaicharoen, N.; Boparai, H. K.; Weber, K. P.; Sharma, P.; Krol, M. M.; Austrins, L.; Peace, C.; Sleep, B. E.; O'Carroll, D. M. Characterization of nZVI mobility in a field scale test. *Environ. Sci. Technol.* **2014**, *48*, 2862−2869.
(61) Johnson, R. L.; Johnson, G. O. B.; Nurmi, J. T.; Tratnyek, P. G. Natural organic matter enhanced mobility of nano zerovalent iron. *Environ. Sci. Technol.* **2009**, *43*, 5455−5460.
(62) Chowdhury, A. I. A.; O'Carroll, D. M.; Xu, Y.; Sleep, B. E. Electrophoresis enhanced transport of nano-scale zero valent iron. *Adv. Water Resour.* **2012**, *40*, 71−82.
(63) Phenrat, T.; Saleh, N.; Sirk, K.; Tilton, R. D.; Lowry, G. V. Aggregation and sedimentation of aqueous nanoscale zerovalent iron dispersions. *Environ. Sci. Technol.* **2007**, *41*, 284−290.
(64) Phenrat, T.; Long, T. C.; Lowry, G. V.; Veronesi, B. Partial Oxidation ("Aging") and Surface Modification Decrease the Toxicity of Nanosized Zerovalent Iron. *Environ. Sci. Technol.* **2009**, *43*, 195−200.
(65) Martín, M.; Montes, F. J.; Galán, M. A. Bubble coalescence at sieve plates: II. Effect of coalescence on mass transfer. Superficial area versus bubble oscillations. *Chem. Eng. Sci.* **2007**, *62*, 1741−1752.
(66) Orvalho, S.; Ruzicka, M. C.; Olivieri, G.; Marzocchella, A. Bubble coalescence: Effect of bubble approach velocity and liquid viscosity. *Chem. Eng. Sci.* **2015**, *134*, 205−216.
(67) Ushikubo, F. Y.; Furukawa, T.; Nakagawa, R.; Enari, M.; Makino, Y.; Kawagoe, Y.; Shiina, T.; Oshita, S. Evidence of the existence and the stability of nano-bubbles in water. *Colloids Surf., A* **2010**, *361*, 31−37.
(68) Vakarelski, I. U.; Manica, R.; Tang, X.; O'Shea, S. J.; Stevens, G. W.; Grieser, F.; Dagastine, R. R.; Chan, D. Y. C. Dynamic interactions between microbubbles in water. *Proc. Natl. Acad. Sci. U.S.A.* **2010**, *107*, 11177−11182.
(69) Stover, R. L.; Tobias, C. W.; Denn, M. M. Bubble coalescence dynamics. *AIChE J.* **1997**, *43*, 2385−2392.
(70) Chang, X.; Henderson, W. M.; Bouchard, D. C. Multiwalled carbon nanotube dispersion methods affect their aggregation, deposition, and biomarker response. *Environ. Sci. Technol.* **2015**, *49*, 6645−6653.
(71) Lin, S.; Wiesner, M. R. Deposition of Aggregated Nanoparticles—A Theoretical and Experimental Study on the Effect of Aggregation State on the Affinity between Nanoparticles and a Collector Surface. *Environ. Sci. Technol.* **2012**, *46*, 13270−13277.

DOI: 10.1021/acs.langmuir.8b02547
Langmuir 2018, 34, 12764−12775